Journal of Nuclear Medicine, published on April 14, 2022 as doi:10.2967/jnumed.121.263079

^{89}Zr-3,2-HOPO-mesothelin antibody PET imaging reflects tumor uptake of mesothelin targeted ^{227}Th-conjugate therapy in mice

Authors: Linda N. Broer[1], Daan G. Knapen[1], Frans V. Suurs[1], Ingrid Moen[2], Danique Giesen[1], Stijn J. H. Waaijer[1], Baard Indrevoll[2], Christine Ellingsen[2], Alexander Kristian[2], Alan S. Cuthbertson[2], Derk-Jan A. de Groot[1], Patricia E. Cole[3], Elisabeth G. E. de Vries[1], Urs B. Hagemann[4], Marjolijn N. Lub-de Hooge[5,6*].

Affiliations: [1]Department of Medical Oncology, University Medical Center Groningen, University of Groningen, Groningen, the Netherlands; [2]Bayer AS, Oslo, Norway; [3]Bayer U.S., LLC, Whippany, NJ; [4]Bayer AG, Berlin, Germany; [5]Department of Clinical Pharmacy and Pharmacology, [6]Department of Nuclear Medicine and Molecular Imaging, University Medical Center Groningen, University of Groningen, Groningen, the Netherlands.

***Corresponding Author:** M.N. Lub-de Hooge, PharmD, PhD, PO Box 30.001, 9700 RB Groningen, The Netherlands +31 50 36 14071 (phone) +31 50 36 14087 (fax) m.n.de.hooge@umcg.nl (e-mail). ORCID iD: https://orcid.org/0000-0002-5390-2791.

First author: Linda N. Broer, PharmD, Groningen, The Netherlands +31 50 36 11817 (phone), l.n.broer@umcg.nl (e-mail).

Data and Materials Availability: Data that support the findings of this study are available from Marjolijn N. Lub-de Hooge upon request.

Running title: PET Imaging for Targeted ^{227}Th Therapy

Keywords: PET imaging, Zirconium-89, Targeted Thorium-227 Therapy, Antibody Conjugate, Mesothelin

Financial support and Disclosure of Potential Conflicts of Interest: This study was supported by a research grant from Bayer provided to E. G. E. de Vries. Payments were made available to her institution (UMCG). Bayer developed and owns the intellectual property rights of 3,2-HOPO-MSLN and ^{227}Th-MSLN. E.G.E. de Vries reports institutional financial support for a consulting and advisory role from Sanofi, Daiichi Sankyo, NSABP, Crescendo Biologics and Cyprus Cancer Research Institute, and institutional financial support for clinical trials or contracted research from Amgen, Genentech, Roche, AstraZeneca, Synthon, Regeneron, Chugai Pharma, CytomX Therapeutics, Servier, Nordic Nanovector, G1 Therapeutics, Radius Health; all outside the submitted work. No other potential conflicts of interest relevant to this article exist.

ABSTRACT

Rationale: Mesothelin targeted thorium-227 conjugate (^{227}Th-MSLN) is a novel targeted alpha therapy developed to treat mesothelin overexpressing cancers. We radiolabeled the same antibody-chelator conjugate with zirconium-89 (^{89}Zr-MSLN) to evaluate if positron emission tomography (PET) imaging with ^{89}Zr-MSLN matches with ^{227}Th-MSLN tumor uptake, biodistribution, and antitumor activity.

Experimental design: Serial PET imaging with protein doses of 4, 20, or 40 µg ^{89}Zr-MSLN and ^{89}Zr-control was performed up to 168 h post tracer injection (pi) in high (HT29-MSLN) and low (BxPc3) mesothelin expressing human tumor-bearing nude mice. ^{89}Zr-MSLN and ^{227}Th-MSLN *ex vivo* tumor uptake and biodistribution were compared at 6 time-points in HT29-MSLN and in medium mesothelin expressing (OVCAR-3) tumor-bearing mice. ^{89}Zr-MSLN PET imaging was performed before ^{227}Th-MSLN treatment in HT29-MSLN and BxPc3 tumor-bearing mice.

Results: ^{89}Zr-MSLN PET imaging showed mean standardized uptake value (SUV_{mean}) in HT29-MSLN tumors of 2.2 ± 0.5. *Ex vivo* tumor uptake was 10.6% ± 2.4% injected dose per gram (%ID/g) at 168 h. ^{89}Zr-MSLN tumor uptake was higher than uptake of ^{89}Zr-control (P = 0.0043). ^{89}Zr-MSLN and ^{227}Th-MSLN showed comparable tumor uptake and biodistribution in OVCAR-3 and HT29-MSLN tumor-bearing mice. Pre-treatment SUV_{mean} was 2.2 ± 0.2 in HT29-MSLN tumors, that decreased in volume upon ^{227}Th-MSLN treatment. BxPc3 tumors showed SUV_{mean} of 1.2 ± 0.3 and remained similar in size after ^{227}Th-MSLN treatment.

Conclusion: ^{89}Zr-MSLN PET imaging reflected mesothelin expression and matched with

^{227}Th-MSLN tumor uptake and biodistribution. Our data support the clinical exploration of ^{89}Zr-MSLN PET imaging together with ^{227}Th-MSLN therapy, both using the same antibody-chelator conjugate.

INTRODUCTION

Despite anticancer therapy advancements, several unmet medical needs remain. For instance, patients with mesothelioma and high-grade serous ovarian cancer would benefit from novel treatment options (1,2).

Recently, targeted alpha therapy has emerged as a potential cancer treatment option. Alpha-particle emitting radionuclides targeted to the tumor enable potent antitumor activity while limiting toxicity to healthy tissues due to their high linear energy transfer and short range in tissue (3,4). Currently, radium-223 (^{223}Ra) dichloride for metastatic castration-resistant prostate cancer is the only approved targeted alpha therapy (5,6). Unlike ^{223}Ra, its progenitor thorium-227 (^{227}Th) forms a stable complex with a 3,2-HOPO chelator conjugated to tumor-associated antigen targeting antibodies (7-9). Targeted ^{227}Th conjugates showed efficacy in mice, including those targeting mesothelin, prostate-specific membrane antigen, CD33, and CD70 (10-14). Tumor-associated antigen binding of targeted ^{227}Th conjugates enables local tumor cell killing via double-strand DNA breaks caused by ^{227}Th decay (9).

Mesothelin is a glycosyl-phosphatidylinositol cell membrane-anchored protein involved in cell-cell adhesion and metastatic spread (15-17). Mesothelin expression by healthy tissues is limited to the peritoneum, pleura, and pericardium. However, it is overexpressed by several human cancers, such as mesothelioma and ovarian cancer (18). Therefore, mesothelin is attractive of targeted cancer therapy, such as antibody-drug conjugates, chimeric antigen receptor T-cells, and targeted radionuclide therapy, currently tested in (pre-)clinical studies (19-22).

Targeted ^{227}Th conjugate, ^{227}Th-MSLN, comprises chelator N-Methyl-3-hydroxypyridine-2-one (3,2-HOPO), covalently attached to fully human anti-mesothelin monoclonal antibody anetumab, stably complexed with alpha particle emitter ^{227}Th (13). The conjugate is only reactive

to human mesothelin. Understanding ^{227}Th-MSLN tumor uptake and biodistribution may be valuable to guide clinical development. Positron emission tomography (PET) can non-invasively visualize biodistribution of monoclonal antibodies, also targeting mesothelin (23-25). We developed a PET-tracer complexing the 3,2-HOPO-MSLN conjugate with ^{89}Zr. By using the same antibody-chelator conjugate we aim to avoid chelator driven differences in pharmacokinetic properties. In mice bearing human mesothelin overexpressing tumors, we evaluated if ^{89}Zr-MSLN PET was able to specifically visualize mesothelin, if this imaging could predict ^{227}Th-MSLN tumor uptake and biodistribution, and whether ^{89}Zr-MSLN tumor uptake matches with ^{227}Th-MSLN antitumor activity.

MATERIALS AND METHODS

Radiolabeling and Quality Control of ^{227}Th-MSLN, ^{89}Zr-MSLN, and ^{89}Zr-control

Radionuclides ^{227}Th and ^{89}Zr were coupled to fully human IgG1 anti-mesothelin monoclonal antibody and an IgG1-isotype control with 3,2-HOPO. This chelator is an octadentate with four bidentate 3,2-HOPO metal-complexation units and a carboxylic arm for monoclonal antibody conjugation, via amide coupling (8). Bayer AG provided conjugates 3,2-HOPO-MSLN and 3,2-HOPO-control with chelator-to-antibody ratios of 0.5. ^{227}Th radiolabeling of 3,2-HOPO-MSLN, resulting in ^{227}Th-MSLN, and quality control was performed as described previously (13). For PET studies, 3,2-HOPO-MSLN and 3,2-HOPO-control were radiolabeled with ^{89}Zr-oxalate (Perkin Elmer) in HEPES 0.5 M, pH 6.7, for 1-2 h at 37 °C. ^{89}Zr-MSLN tended to form radioactive dimers. For the 4 µg dose, the radioactive dimer formation was 10% at a 0.1 mg/mL antibody concentration, with protein desalting purification in 10 mM histidine and 130 mM glycine at pH 7.4 in water. The 20 and 40 µg dose preparation required higher concentrations of 0.2 and 0.4 mg/mL antibody

during radiolabeling, resulting in 30% and 60% radioactive dimers, respectively. The effect of 60% and 10% radioactive dimer content on ^{89}Zr-MSLN biodistribution was compared at the 4 µg dose. To induce 60% dimers at this dose, an additional radiolabeling was performed at 0.4 mg/mL antibody with purification via Vivaspin centrifugation in 0.9% NaCl. For ^{89}Zr-MSLN quality control, size exclusion ultra-performance liquid chromatography was used with a TSK-Gel SW column G3000SWXL 5 µm, 7.8 mm (Joint Analytical Systems), elution buffer phosphate-buffered saline (140.0 mM NaCl, 9.0 mM Na_2HPO_4, 1.3 mM NaH_2PO_4) and 0.7 mL/min flow rate (absorbance detection: 280 nm; radioactivity detection). Radiochemical purity was assessed by trichloroacetic acid precipitation assay (26). To determine the immunoreactive fraction a 10-fold molar excess recombinant mesothelin extracellular domain (R&D Systems, #3265-MS-050) was added to ^{89}Zr-MSLN, assessed by radioactivity chromatogram overlay peak intersection of bound ^{89}Zr-MSLN vs. unbound ^{89}Zr-MSLN.

Cell Lines

BxPc3 human pancreatic and OVCAR3 human ovarian cancer cells were obtained from American Type Culture Collection and HT29-MSLN mesothelin transfected human colon cancer cells were obtained from Bayer AG, generated at Natural and Medical Sciences Institute (respectively 4,200; 37,877 and 242,413 mesothelin molecules per cell) (13). All cell lines were mycoplasma negative. The genetic origin of the cell lines was authenticated by BaseClear using short tandem repeat profiling. BxPc3 and OVCAR-3 cells were cultured in DMEM/Ham's F12 and HT29-MSLN cells in RPMI, 600 µg/mL hygromycin B. All cells were cultured in 10% fetal calf serum, 1% penicillin/streptomycin, and incubated at 37 °C, with 5% CO_2 in a humidified incubator.

Animal Studies

Animal experiments were performed conform animal welfare laws in the Netherlands and Norway. Female nude mice, 4-10 weeks of age and 25-35 g, received 200 µg irrelevant IgG2A (Sigma-Aldrich) within 24 h before ^{89}Zr-MSLN, ^{89}Zr-control, or ^{227}Th-MSLN injection to limit unspecific uptake in liver and spleen (27). A 20 µg dose was used as standard dose, in line with published data (13). To investigate ^{89}Zr-MSLN dose-effect, 4 and 20 µg ^{89}Zr-MSLN were applied, equalling 0.14 mg/kg and 0.75 mg/kg in (13) with an additional dose of 40 µg. Only a 20 µg nonspecific ^{89}Zr-control was used, not expecting a dose-effect. Tumor volumes were measured with caliper and calculated with formula 'long side*short side^2/2', expressed as mm^3. Mice with similar tumor sizes were balanced out between groups. Comparison of *ex vivo* tissue uptake between ^{89}Zr-MSLN and ^{227}Th-MSLN was performed in Female Balb/c nude-Foxn1^{nu}(Janvier France). In this experiment inclusion of 25-30 mm^3 tumor sizes was accepted given the challenging tumor growth of the OVCAR-3 model. For PET experiments, Female NMRI-Foxn1^{nu} mice (Taconic Europe) were used, enabling direct comparison with published data (13). To reliably quantify PET data, the inclusion criterion for the imaging studies was a tumor size of >150 mm^3. Therefore, the OVCAR-3 tumor model was excluded for PET imaging.

To investigate ^{89}Zr-MSLN tumor and healthy tissue uptake, dose-effect and radioactive dimers, NMRI-Foxn1^{nu} mice were inoculated with 1.0 x 10^6 HT29-MSLN cells 14 days or 2.5 x 10^6 BxPc3 cells 21 days before start of PET studies. HT29-MSLN tumor-bearing mice received 20 µg ^{89}Zr-MSLN or ^{89}Zr-control (3-4 MBq, n = 6). BxPc3 tumor-bearing mice received 4 µg, 20 µg, or 40 µg ^{89}Zr-MSLN, or 20 µg ^{89}Zr-control (1-5 MBq, n = 6). Given radioactive dimer formation, we did not exceed 40 µg. Only 20 µg and 40 µg dose groups could undergo PET imaging 24, 72, and 168 h post-injection (pi). *Ex vivo* biodistribution was performed for all groups at 168 h pi. The effect of radioactive dimers on tissue uptake was tested at 4 µg ^{89}Zr-MSLN with 10% vs 60%

radioactive dimers in BxPc3 tumor-bearing mice. Female Balb/c nude-Foxn1^{nu} mice were inoculated with 1.0 x 10^6 HT29-MSLN cells 5 days or 5.0 x 10^6 OVCAR-3 cells 28 days before comparison of *ex vivo* tissue uptake of ^{89}Zr-MSLN vs ^{227}Th-MSLN. Mice received 20 µg ^{89}Zr-MSLN (0.20 MBq) or 20 µg ^{227}Th-MSLN (0.015 MBq), and sacrificed 0.5, 2, 6, 24, 72 and 168 h pi (n = 4-5). To study if ^{89}Zr-MSLN PET tumor uptake coincided with ^{227}Th-MSLN antitumor activity, BxPc3 and HT29-MSLN tumor-bearing NMRI-Foxn1^{nu} mice underwent ^{89}Zr-MSLN PET imaging 168 h pi (4 MBq, 20 µg) and received 0.75 mg/kg, 500 kBq/kg ^{227}Th-MSLN 5 days after imaging *(n* = 7-8, no treatment: *n* = 2). In this time frame no changes in mesothelin tumor expression were to be expected. Tumor sizes were measured untill 21 days after treatment.

Mice were imaged with a Focus 220 PET scanner (CTI Siemens). PET data was reconstructed, corrected for decay, random coincidences, scatter, and attenuation. Tumor and heart uptake were quantified with PMOD software version 4.004, as mean standardized uptake value (SUV_{mean}). *Ex vivo* blood and tissues were weighed and radioactivity measured in a Wizard gamma counter (PerkinElmer, UMCG) or germanium detector (Ortex, Bayer AS). *Ex vivo* uptake was expressed as percentage injected dose per gram (%ID/g).

***Ex vivo* Analysis of Plasma and Tumor**

Tracer integrity of ^{89}Zr-MSLN in plasma of mice sacrificed at 168 h pi was studied by sodium dodecyl sulfate-polyacrylamide gel electrophoresis. Mini-Protean® TGX™ precast protein gels 4-15% (BioRad) were loaded with 80 µg plasma protein. A control sample including intact tracer and free ^{89}Zr was generated by storing ^{89}Zr-MSLN at room temperature (RT) for a week. Gels ran for 30-45 min at 100 V. Formalin-fixed tumor tissues were paraffin-embedded and sliced into 4 µm sections. Gels and tumor sections were exposed overnight to a multipurpose phosphor plate (Perkin Elmer) at -20 °C and captured with Cyclone® phosphor imager (Perkin Elmer).

Mesothelin immunohistochemistry was executed on the autoradiography tumor sections, as described earlier (28). Ventana Discovery autostainer was used with DAB detection chemistry with anti-rabbit-HQ and anti-MSLN antibody (clone SP74, Spring Biosciences) at 0.25 µg/mL. Sections were fixed at 4ºC for 5 min, air-dried, and washed with double-distilled H_2O before incubation with DAKO blocking solution (10 min, RT). After washing, primary antibody was detected with HRP-labeled-anti-mouse polymer (Dako) and DAB solution. Hematoxylin-eosin staining was performed on adjacent tumor sections. Digital scans were acquired by a Hamamatsu NanoZoomer 2.0-HT multi-slide scanner and analyzed with NanoZoomer Digital Pathology viewer software.

Statistical Analysis

Similarity between two groups was analyzed using a Mann-Whitney U test. In case of multiple groups or time-points, a Bonferroni multiple comparison correction was applied. All data are presented ± standard deviation. All statistical tests were performed in GraphPad Prism 8, and *P*-values < 0.05 were considered significant.

RESULTS

Quality control ^{89}Zr-MSLN

^{89}Zr-MSLN was produced with a radiolabeling efficiency of 64% ± 10%, a radiochemical purity of 98% ± 1%, and with 4% ± 1% antibody dimers and 15% ± 2% radiolabeled dimers (n = 6) (Suppl. Fig. 1A). The immunoreactive fraction was 0.8 (Suppl. Fig. 1B). We observed by radioactive detection that ^{89}Zr-MSLN tended to dimerize, not observed at 280 nm. Favorable and unfavorable conditions are shown in Suppl. Table 1. Radiolabeling conditions and quality control results of the experiments are shown in Suppl. Fig. 1C,D and Suppl. Table 2.

Tumor Uptake and Biodistribution of ^{89}Zr-MSLN

PET evaluation of ^{89}Zr-MSLN in HT29-MSLN tumor-bearing mice showed 1.8-fold higher ^{89}Zr-MSLN tumor uptake and tumor-to-blood ratio than ^{89}Zr-control (SUV_{mean} of 2.2 ± 0.5 vs. 1.2 ± 0.2, 168 h pi; P = 0.0043; Fig. 1A,B). *Ex vivo* biodistribution confirmed PET data, showing 2.5-fold higher tumor uptake of ^{89}Zr-MSLN than ^{89}Zr-control at 168 h (10.6% ± 2.4% vs 4.2% ± 0.7% ID/g; P = 0.0043), while uptake in all other tissues was similar (Fig. 2). No low molecular weight species of ^{89}Zr-MSLN or free ^{89}Zr were present in blood 168 h pi (Suppl. Fig. 1E). Autoradiography showed mesothelin specific ^{89}Zr-MSLN tumor uptake compared with ^{89}Zr-control (Fig. 3, Suppl. Fig. 2A,B).

Dose-Effect of ^{89}Zr-MSLN on Tumor Uptake and Biodistribution

In vivo, ^{89}Zr-MSLN BxPc3 tumor uptake and tumor-to-blood ratios were lower than in HT29-MSLN tumors. ^{89}Zr-MSLN BxPc3 tumor uptake and tumor-to-blood ratios were similar between 20 µg and 40 µg (SUV_{mean} 1.6 ± 0.2 vs. 1.9 ± 0.3) and higher than 20 µg ^{89}Zr-control (SUV_{mean} 1.1 ± 0.2, Fig. 4 A,B). *Ex vivo,* ^{89}Zr-MSLN tumor and liver uptake were higher at 40 vs 4 µg 168 h pi. In addition, 60% vs 10% radioactive dimers at 4 µg ^{89}Zr-MSLN showed higher tumor (10.0% ± 2.2% vs 6.1% ± 1.7% ID/g) and liver uptake (8.8% ± 1.4% vs 4.9% ± 1.2% ID/g). Excretion rate was not affected by radioactive dimers. Bone uptake was mainly in cortical bone and not in bone marrow (Suppl. Fig. 3A-D).

^{89}Zr-MSLN vs ^{227}Th-MSLN Tumor Uptake and Biodistribution

Ex vivo OVCAR3 and HT29-MSLN tumor uptake of ^{89}Zr-MSLN and ^{227}Th-MSLN was comparable except at 168 h pi, revealing lower ^{89}Zr-MSLN HT29-MSLN tumor uptake (33.1% ± 9.0% vs. 89.8% ± 26.3%ID/g, P = 0.016, Fig. 5A). Tumor-to-blood ratios were similar for ^{89}Zr-

MSLN and ^{227}Th-MSLN in both models (Fig. 5B). ^{89}Zr-MSLN liver uptake was higher than ^{227}Th-MSLN up to 24 h in HT29-MSLN tumor-bearing mice, but not at 72 and 168 h, the clinically relevant timepoints. ^{89}Zr-MSLN uptake in femur was higher than ^{227}Th-MSLN from 24 to 168 h in both models, e.g., 12.3% ± 1.3% ID/g vs 4.9% ± 0.6% ID/g, 168 h pi in the HT29-MSLN tumor-bearing mice, resulting in lower blood and kidney levels at 72 h and 168 h (Suppl. Fig. 4A-B).

^{89}Zr-MSLN PET before ^{227}Th-MSLN Treatment

^{89}Zr-MSLN PET imaging before ^{227}Th-MSLN treatment revealed 1.8-fold higher tumor SUV_{mean} in HT29-MSLN than in BxPc3 tumors (2.2 ± 0.2 vs 1.2 ± 0.3; P = 0.0003, Fig. 6A,B). Due to ^{227}Th's 18.7 days half-life, treatment effect is not observed in the first 9 days. From day 9 until day 21 after ^{227}Th-MSLN administration, HT29-MSLN tumors decreased 0.7 ± 0.1-fold in volume (from 432.4 ± 131.2 mm^3 to 317.4 ± 130.1 mm^3). Tumors of untreated mice grew individually 1.3-fold and 1.7-fold. In the same time frame, BxPc3 tumors did not grow after ^{227}Th-MSLN administration (1.0 ± 0.3-fold, 310.2 ± 166.5 mm^3 at day 9 and 288.3 ± 112.3 mm^3 at day 21) while tumors of untreated animals individually grew each 1.4-fold (Fig. 7A,B). Absolute tumor growth is shown in Suppl. Fig. 5. BxPc3 tumors of untreated- vs ^{227}Th-MSLN-treated animals were slightly larger at day 0. Therefore, tumor sizes were normalized to the size at day 0 (29). ^{227}Th-MSLN treatment increased DNA double-strand breaks compared to tumors of untreated mice, confirming the molecular mode of action of ^{227}Th-MSLN (Suppl. Fig. 6 A,B).

DISCUSSION

This study shows that ^{89}Zr-MSLN PET imaging reflects ^{227}Th-MSLN tumor uptake and biodistribution in mice bearing human mesothelin overexpressing tumors. We show the dual-use of an antibody-chelator conjugate, 3,2-HOPO-MSLN, radiolabeled with ^{89}Zr for PET imaging, and with ^{227}Th for targeted alpha therapy as a theranostic. Even though some studies show direct

molecular imaging of ^{227}Th, this remains a challenge due to the low abundance of measurable photons in ^{227}Th's decay chain (30). Studies in patients and mice showed ^{89}Zr PET's theranostic potential for beta particle emitting therapeutic radionuclides, such as lutetium-177 and yttrium-90 (31,32). Therefore, we hypothesized that ^{89}Zr might serve as a PET surrogate radioisotope for alpha particle emitter ^{227}Th as well. Estimating ^{227}Th-MSLN whole-body distribution with ^{89}Zr-MSLN PET before treatment may be of value to guide clinical development. In addition, this study encourages ^{89}Zr-MSLN PET exploration to select patients, and predict ^{227}Th-MSLN efficacy. Moreover, PET imaging with ^{89}Zr may be amenable to other targeted alpha therapies.

^{89}Zr-MSLN tumor uptake might correlate with response to ^{227}Th-MSLN. However, we did not use the isogenic cell systems required to exclude differences in sensitivity to ^{227}Th-MSLN. We did not perform tumor biopsies to assess whether changes in mesothelin expression occurred in the 5-day time frame between PET scan and start of treatment. A change is unlikely as tumor growth was relatively consistent. We observed a trend in antitumor activity of ^{227}Th-MSLN comparable with the earlier *in vivo* study (13). A firm conclusion on predicting ^{227}Th-MSLN antitumor activity is precluded given the low number of animals in the control groups.

Variability in ^{89}Zr-MSLN and ^{227}Th-MSLN tumor uptake may have been a result of small tumors in the *ex vivo* biodistribution comparison. Higher ^{89}Zr-MSLN bone uptake might be explained by dissociated ^{89}Zr from 3,2-HOPO, tending to accumulate in growing bone cone in young mice, not seen in humans (33,34). *Ex vivo* blood samples at 168 h showed intact ^{89}Zr-MSLN, indicating that the tracer available in the circulation for tissue uptake is intact. This suggests that free ^{89}Zr clears from the blood immediately into cortical bone. Although desferrioxamine-based chelators are commonly used to complex ^{89}Zr with, HOPO-based chelators are a proven alternative (35,36). To avoid chelator-driven discrepancies in pharmacokinetics between ^{89}Zr-MSLN and ^{227}Th-MSLN (37,38) we developed the PET-tracer using the same 3,2-HOPO-MSLN conjugate

with the additional advantage of having the intermediate product clinical-grade right at hand. We showed in mice that ^{89}Zr-MSLN uptake can predict tumor targeting of ^{227}Th-MSLN. In patients, ^{89}Zr-MSLN PET imaging might detect mesothelin-positive lesions in mesothelioma, ovarian and pancreatic cancer and clarify if the antibody can reach these lesions. Yet, calculating an exact ^{227}Th radiation dose per organ is limited by the observed ^{89}Zr-MSLN bone uptake. For potential dosimetry purposes, we should aim to improve *in vivo* stability of HOPO-based ^{89}Zr chelators.

Higher liver uptake of high radioactive dimer content ^{89}Zr-MSLN indicates faster clearance of dimers and aggregates than monomers (39). Higher tumor uptake could be explained by increased retention at the target-binding site due to an avidity effect (40) combined with enhanced permeability and retention effect (41). Higher tumor uptake at 40 vs 4 μg total antibody dose may, therefore, most likely be a dimer- instead of a dose-effect. Dimerization appears specific for ^{89}Zr-3,2-HOPO, since the control antibody revealed similar radioactive dimer content, not observed in combination with ^{227}Th to the same extent (13). In a clinical setting, the specification should be set at < 15%. This is feasible with the optimized radiolabeling procedure that we describe.

CONCLUSION

In conclusion, our study reveals the potential of ^{89}Zr-MSLN PET to predict ^{227}Th-MSLN tumor uptake and biodistribution. Furthermore, it addresses the potential of ^{89}Zr-MSLN PET as a tool to estimate ^{227}Th-MSLN antitumor activity. Our data support clinical investigation of ^{89}Zr-MSLN PET imaging in combination with ^{227}Th-MSLN therapy.

ACKNOWLEDGMENTS

We would like to thank Manuela Brand for the immunohistochemistry and immunofluorescent staining (Bayer AG) and Linda Pot-de Jong for assisting with the animal experiments (Department of Medical Oncology, University Medical Center Groningen).

KEY POINTS

Question: Could ^{89}Zr-MSLN PET imaging predict ^{227}Th-MSLN behavior?

Pertinent findings: ^{89}Zr-MSLN PET imaging shows similar tumor uptake and biodistribution as ^{227}Th-MSLN in mesothelin expressing tumor-bearing nude mice.

Clinical implications: These data support theranostic potential of ^{89}Zr-MSLN PET imaging to guide ^{227}Th-MSLN therapy in patients.

REFERENCES

1. Christoph DC, Eberhardt WE. Systemic treatment of malignant pleural mesothelioma: new agents in clinical trials raise hope of relevant improvements. *Curr Opin Oncol*. 2014;26:171–181.
2. Herzog TJ, Monk BJ. Bringing new medicines to women with epithelial ovarian cancer: what is the unmet medical need? *Gynecol Oncol Res Pract*. 2017;4:13.
3. Parker C, Lewington V, Shore N, et al. Targeted alpha therapy, an emerging class of cancer agents: A review. *JAMA Oncol.* 2018;4:1765–1772.
4. Guerra Liberal FDC, O'Sullivan JM, McMahon SJ, Prise KM. Targeted alpha therapy: Current clinical applications. *Cancer Biother Radiopharma*. 2020;35:404-417.
5. Parker C, Nilsson S, Heinrich D, et al. Alpha emitter radium-223 and survival in metastatic prostate cancer. *N Engl J Med.* 2013;369:213–223.
6. Kratochwil C, Haberkorn U, and Giesel FL. Radionuclide therapy of metastatic prostate cancer. *Sem Nucl Med.* 2019; 49:313-325.
7. Ramdahl T, Bonge-Hansen HT, Ryan OB, et al. An efficient chelator for complexation of thorium-227. *Bioorg Med Chem Lett.* 2016;26:4318–4321.
8. Deblonde G, Lohrey T, Booth C, et al. Solution thermodynamics and kinetics of metal complexation with a hydroxypyridinone chelator designed for thorium-227 targeted alpha therapy. Inorg Chem. 2018;57:14337–14346.
9. Hagemann UB, Wickstroem K, Hammer S, et al. Advances in precision oncology: Targeted thorium-227 conjugates as a new modality in targeted alpha therapy. *Cancer Biother Radiopharm.* 2020;00:1-14.

10. Dahle J, Borrebaek J, Jonasdottir TJ, et al. Targeted cancer therapy with a novel low-dose rate alpha-emitting radioimmunoconjugate. *Blood.* 2007;110:2049–2056.
11. Hagemann UB, Wickstroem K, Wang E, et al. In vitro and in vivo efficacy of a novel CD33-targeted thorium-227 conjugate for the treatment of acute myeloid leukemia. *Mol Cancer Ther.* 2016;15:2422–2431.
12. Hagemann UB, Mihaylova D, Uran SR, et al. Targeted alpha therapy using a novel CD70 targeted thorium-227 conjugate in in vitro and in vivo models of renal cell carcinoma. *Oncotarget.* 2017;8:56311–56326.
13. Hagemann UB, Ellingsen C, Schuhmacher J, et al. Mesothelin-targeted thorium-227 conjugate (MSLN-TTC): preclinical evaluation of a new targeted alpha therapy for mesothelin-positive cancers. *Clin Cancer Res*. 2019;25:4723-4734.
14. Hammer S, Hagemann UB, Kolbe-Zitzmann S, et al. Preclinical efficacy of a PSMA-targeted thorium-227 conjugate (PSMA-TTC), a targeted alpha therapy for prostate cancer. *Clin Cancer Res.* 2020;28:198596.
15. Bera TK, Pastan I. Mesothelin is not required for normal mouse development or reproduction. *Mol Cell Biol*. 2000;20:2902–2906.
16. Chen SH, Hung WC, Wang P, Paul C, Konstantopoulos K. Mesothelin binding to CA125/MUC16 promotes pancreatic cancer cell motility and invasion via MMP-7 activation. *Sci Rep.* 2013;3:1870.
17. Rump A, Morikawa Y, Tanaka M, et al. Binding of ovarian cancer antigen CA125/MUC16 to mesothelin mediates cell adhesion. *J Biol Chem.* 2004;279:9190–9198.
18. Hassan R, Thomas A, Alewine C, Le TL, Jaffee EM, Pastan I. Mesothelin immunotherapy for cancer: ready for prime time? *J Clin Oncol.* 2016 Dec;34:4171–4179.

19. Morello A, Sadelain M, Adusumilli PS. Mesothelin-targeted CARs: driving T cells to solid tumors. *Cancer Discov.* 2016;6:133–146.

20. Zhao XY, Subramanyam B, Sarapa N, Golfier S, Dinter H. Novel antibody therapeutics targeting mesothelin in solid tumors. *Clin Cancer Drugs.* 2016; 3:76–86.

21. Quanz M, Hagemann U, Zitzmann-Kolbe S, et al. Anetumab ravtansine inhibits tumor growth and shows additive effect in combination with targeted agents and chemotherapy in mesothelin-expressing human ovarian cancer models. *Oncotarget.* 2018;9: 34103–34121.

22. Hassan R, Blumenschein GR Jr, Moore KN, Santin AD, Kindler HL. First-in-human, multicenter, phase I dose-escalation and expansion study of anti-mesothelin antibody-drug conjugate anetumab ravtansine in advanced or metastatic solid tumors. *J Clin Oncol.* 2020;38:1824-1835.

23. Gebhart G, Lamberts LE, Wimana Z, et al. Molecular imaging as a tool to investigate heterogeneity of advanced HER2-positive breast cancer and to predict patient outcome under trastuzumab emtansine (T-DM1): The ZEPHIR trial. *Ann Oncol.* 2016;27:619–624.

24. Lamberts LE, Menke-van der Houven van Oordt CW, ter Weele EJ, et al. ImmunoPET with anti-mesothelin antibody in patients with pancreatic and ovarian cancer before anti-mesothelin antibody–drug conjugate treatment. *Clin Cancer Res.* 2016;22:1642-1652

25. Bensch F, van der Veen EL, Lub-de Hooge MN, et al. ^{89}Zr-atezolizumab imaging as a non-invasive approach to assess clinical response to PD-L1 blockade in cancer. *Nat Med.* 2018;24:1852–1858.

26. Nagengast WB, de Vries EG, Hospers GA, et al. In vivo VEGF imaging with radiolabeled bevacizumab in a human ovarian tumor xenograft. *J Nucl Med.* 2007;48:1313-1319.

27. Reddy N, Ong GL, Behr TM, Sharkey RM, Goldenberg DM, Mattes MJ. Rapid blood clearance of mouse IgG2a and human IgG1 in many nude and nu/þ mouse strains is due to low IgG2a serum concentrations. *Cancer Immunol Immunother.* 1998;46:25–33.

28. Golfier S, Kopitz C, Kahnert A, et al. Anetumab ravtansine: A novel mesothelin-targeting antibody–drug conjugate cures tumors with heterogeneous target expression favored by bystander Effect. *Mol Cancer Ther.* 2014;13:1537-1548.

29. Hather G, Liu R, Bandi S, et al. Growth rate analysis and efficient experimental design for tumor xenograft studies *Cancer Informatics* 2014;13: 65–72.

30. Murray I, Rojas B, Gear J, Callister R, Cleton A, Flux GD. Quantitative dual-isotope planar imaging of thorium-227 and radium-223 using defined energy windows. *Cancer Biother Radiopharm.* 2020; 35: 530–539.

31. Perk LR, Visser GWM, Vosjan MJWD, et al. ^{89}Zr as a PET surrogate radioisotope for scouting biodistribution of the therapeutic radiometals ^{90}Y and ^{177}Lu in tumor-bearing nude mice after coupling to the internalizing antibody cetuximab. *J Nucl Med.* 2005;46:1898–1906.

32. Rizvi SNF, Visser OJ, Vosjan MJWD, et al. Biodistribution, radiation dosimetry and scouting of ^{90}Y-ibritumomab tiuxetan therapy in patients with relapsed B-cell non-Hodgkin's lymphoma using ^{89}Zr-ibritumomab tiuxetan and PET. *Eur J Nucl Med Mol Imaging.* 2012;39:512–520.

33. Deri MA, Zeglis BM, Francesconi LC, Lewis JS. PET imaging with ^{89}Zr: from radiochemistry to the clinic. *Nucl Med Biol.* 2013;40:3–14.

34. Bensch F, Smeenk MM, van Es SC, et al. Comparative biodistribution analysis across four different ^{89}Zr-monoclonal antibody tracers-The first step towards an imaging warehouse. *Theranostics.* 2018;8:4295-304.

35. Tinianow JN, Pandya DN, Pailloux SL, et al. Evaluation of a 3-hydroxypyridin-2-one (2,3-HOPO) based macrocyclic chelator for $^{89}Zr^{4+}$ and its use for immunoPET imaging of HER2

positive model of ovarian carcinoma in mice. *Theranostics.* 2016;6:511–521.

36. Deri MA, Ponnala S, Kozlowski P, et al. HOPO p-SCN-Bn-HOPO: A superior bifunctional chelator for ^{89}Zr immunoPET. *Bioconjug Chem.* 2015;26:2579−2591.

37. Bhatt NB, Pandya DN, Wadas TJ. Recent advances in zirconium-89 chelator development. *Molecules.* 2018;23: 638.

38. Heskamp S, Raavé R, Boerman O, Rijpkema M, Goncalves V, and Denat F. ^{89}Zr-immuno-positron emission tomography in oncology: state-of-the-art ^{89}Zr radiochemistry. *Bioconjugate Chem.* 2017;28:2211–2223.

39. Hotzel I, Theil FP, Bernstein LJ, et al. A strategy for risk mitigation of antibodies with fast clearance. *MAbs.* 2012;4:753–760.

40. Kortt AA, Dolezal O, Power BE, Hudson PJ. Dimeric and trimeric antibodies: high avidity scFvs for cancer targeting. *Biomol Eng.* 2001;18:95-108.

41. Kalyane D, Raval N, Maheshwari R, Tambe V, Kalia K, Tekade R. Employment of enhanced permeability and retention effect (EPR): Nanoparticle-based precision tools for targeting of therapeutic and diagnostic agent in cancer. *Mater Sci Eng C*. 2019;98:1252–1276.

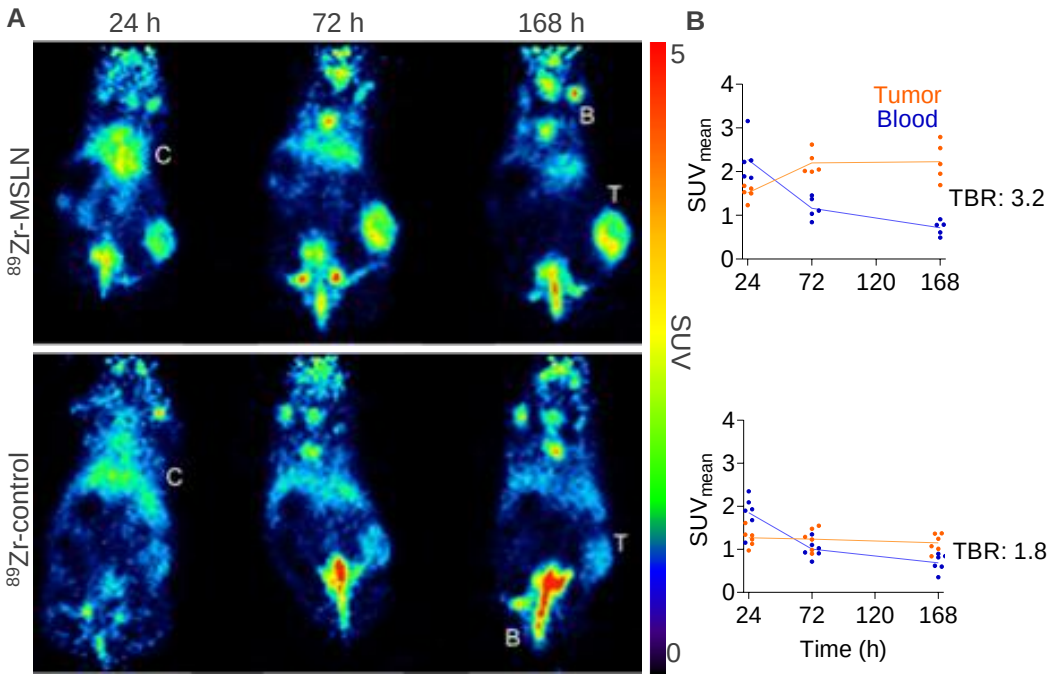

FIGURE 1. *In vivo* tumor uptake and biodistribution of ^{89}Zr-MSLN

HT29-MSLN tumor-bearing mice (*n* = 6 per group) **A** representative coronal PET images at 24 h, 72 h, and 168 h after 20 µg ^{89}Zr-MSLN and 20 µg ^{89}Zr-control (3-4 MBq). Uptake is presented as standardized uptake value (SUV). **B** PET quantification of ^{89}Zr-MSLN and ^{89}Zr-control uptake in tumor and blood at 24 h, 72 h and 168 h pi. ^{89}Zr-MSLN and ^{89}Zr-control uptake are shown as mean standardized uptake value (SUV_{mean}) ± standard deviation (SD). Tumor-to-blood ratio is indicated at 168 h. C: circulation, B: bone, T: tumor.

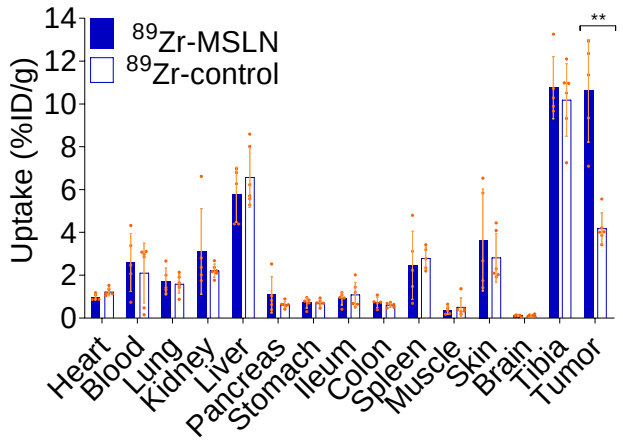

FIGURE 2. *Ex vivo* Tumor uptake and biodistribution of ^{89}Zr-MSLN

HT29-MSLN tumor-bearing mice (n = 6 per group) *Ex vivo* tumor and healthy tissue uptake of 20 µg ^{89}Zr-MSLN and 20 µg ^{89}Zr-control at 168 h pi. Data is presented as percentage injected dose per gram tissue (%ID/g), as mean ±SD, The ^{89}Zr-MSLN and ^{89}Zr-control batches each contained 30 % radioactive dimers. **: $P < 0.01$, *: $P < 0.05$, ns: not significant. C: circulation, B: bone, T: tumor, L: liver.

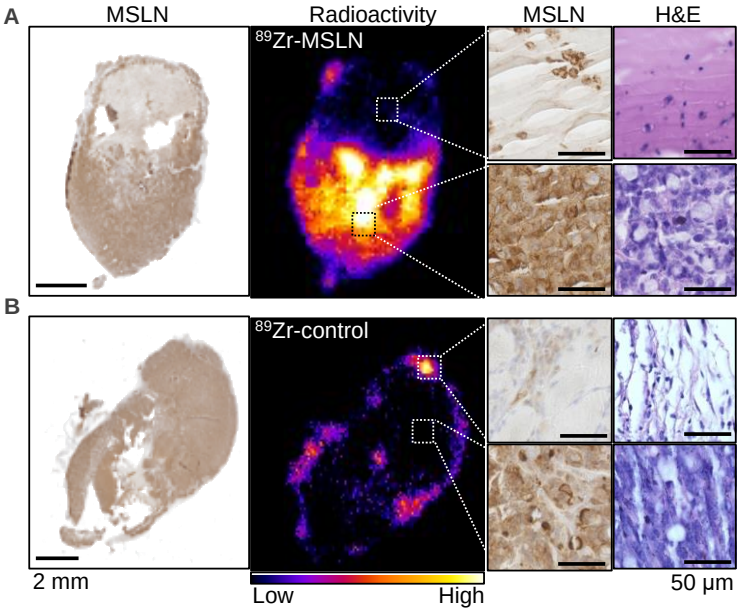

FIGURE 3. Intratumoral ^{89}Zr-MSLN distribution

Mesothelin immunohistochemistry, autoradiography, and hematoxylin/eosin of HT29-MSLN and formalin-fixed, paraffin-embedded tumor sections, that received **A** ^{89}Zr-MSLN or **B** ^{89}Zr-control. Mesothelin immunohistochemistry and autoradiography are performed on the same and hematoxylin/eosin on an adjacent tumor section. Radioactivity in A and B is simultaneously scaled, shown from high to low ^{89}Zr signal intensity. Representative data shown (n = 3-5, rest is shown in Suppl. Fig. 2).

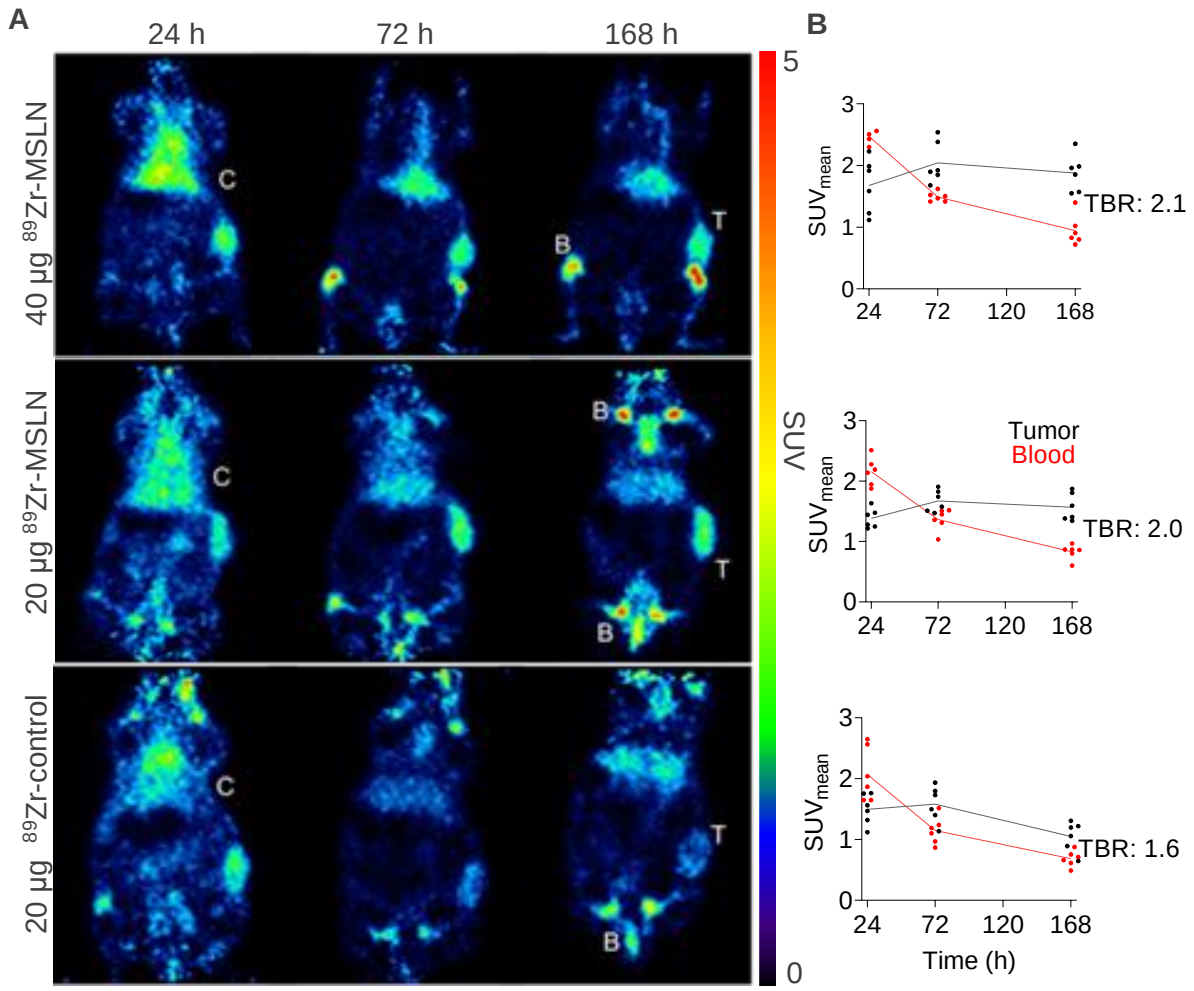

FIGURE 4. Dose-effect of ^{89}Zr-MSLN on tumor uptake and biodistribution

BxPc3 tumor-bearing mice (*n* = 5-6 per group) **A** representative coronal PET images of 40 µg and 20 µg ^{89}Zr-MSLN and 20 µg ^{89}Zr-control at 24 h, 72 h, and 168 h pi. Uptake is presented as standardized uptake value (SUV) and **B** quantification of tumor and blood at 24 h, 72 h and 168 h pi, shown as mean standardized uptake value (SUV_{mean}) ± standard deviation (SD). Tumor-to-blood ratio is indicated at 168 h. Tumor-to-blood ratio is indicated at 168 h, pi: post injection, C: circulation, B: bone, T: tumor.

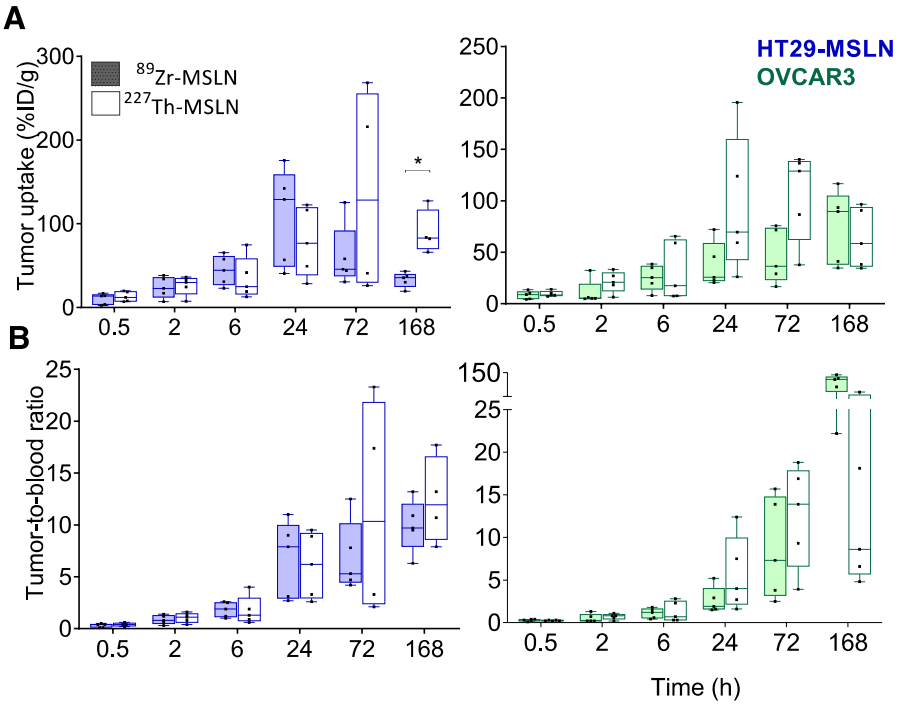

FIGURE 5. Tumor uptake of ^{89}Zr-MSLN compared with ^{227}Th-MSLN

A HT29-MSLN tumor uptake and **B** OVCAR3 Tumor uptake and **C** + **D** respective tumor-to-blood ratios, of 20 µg ^{89}Zr-MSLN (0.20 MBq) vs 20 µg ^{227}Th-MSLN (0.015 MBq) total antibody dose at 0.5, 2, 6, 24, 72, and 168 h. Data is presented as median percentage injected dose per gram tissue (%ID/g) and interquartile range including single data points. *: $P < 0.05$ with Bonferroni correction.

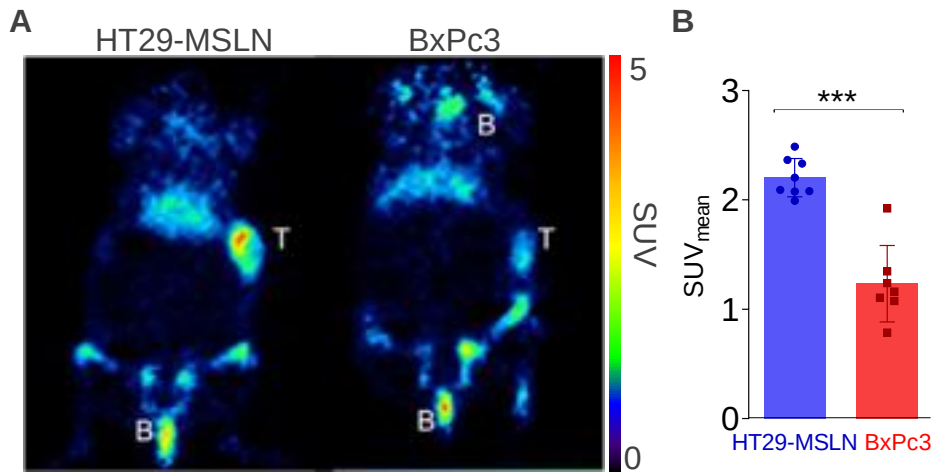

FIGURE 6. ^{89}Zr-MSLN PET before ^{227}Th-MSLN treatment

A Representative coronal PET images of HT29-MSLN and BxPc3 tumor-bearing mice 168 h after 20 µg ^{89}Zr-MSLN, tumor uptake presented as standardized uptake value (SUV). **B** Quantification of ^{89}Zr-MSLN in HT29-MSLN and BxPc3 tumors at 168 h pi (n = 7-8 per group). ^{89}Zr-MSLN uptake is shown as mean standardized uptake value (SUV_{mean}) ± standard deviation (SD), including single data points. ***: $P < 0.001$. B: bone, T: tumor, L: liver.

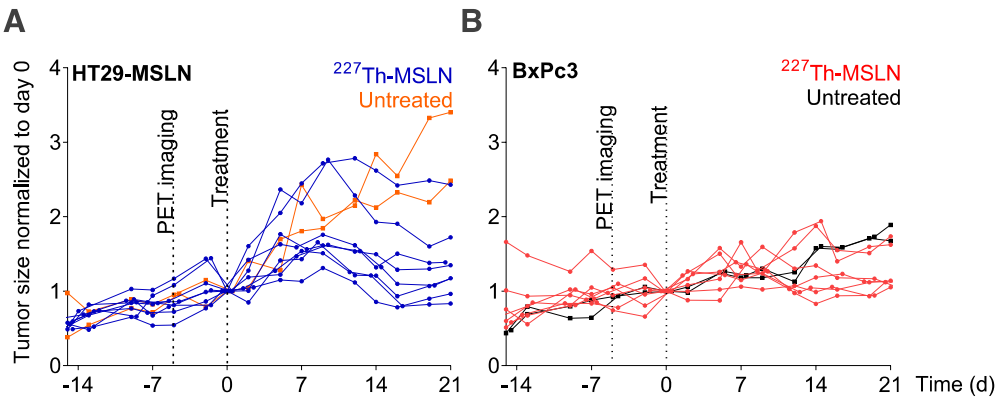

FIGURE 7. Tumor growth after ^{227}Th-MSLN treatment

A Tumor growth after ^{227}Th-MSLN treatment, 0.75 mg/kg, 500 kBq/kg of HT29-MSLN tumor-bearing mice (n = 8) **B** and BxPc3 tumor-bearing mice (n = 7) and per model n = 2 untreated mice, normalized to day 0. For absolute tumor sizes, see Suppl. Fig. 5.

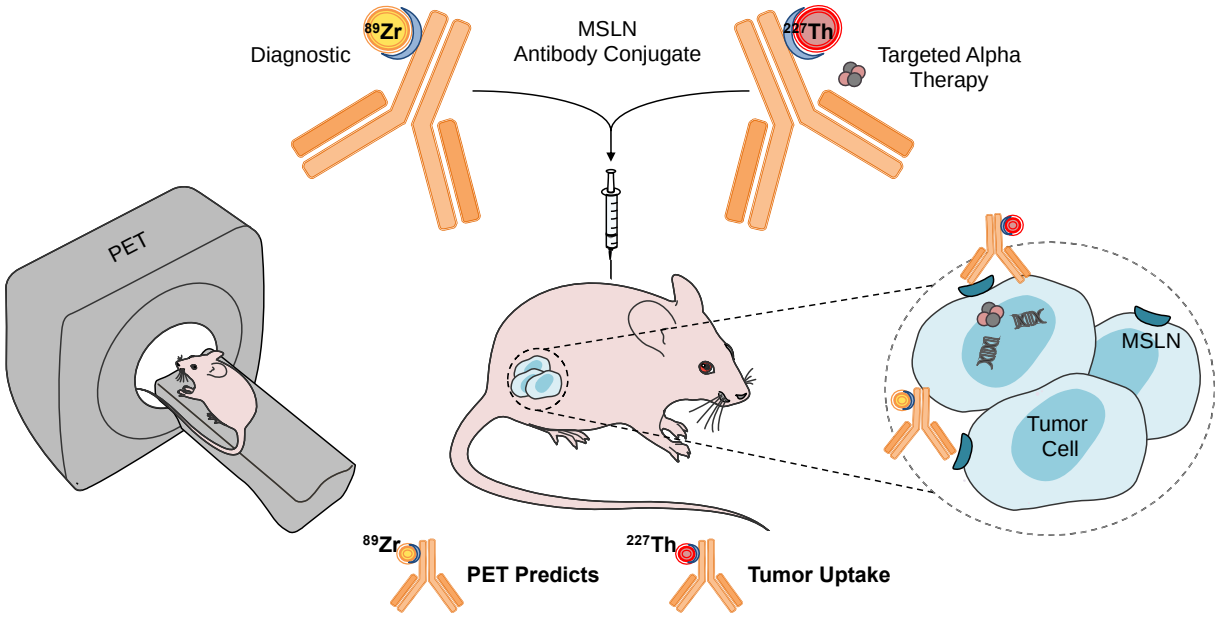

GRAPGICAL ABSTRACT MSLN: mesothelin, ^{89}Zr: zirconium-89, ^{227}Th: thorium-227, PET: positron emission tomography

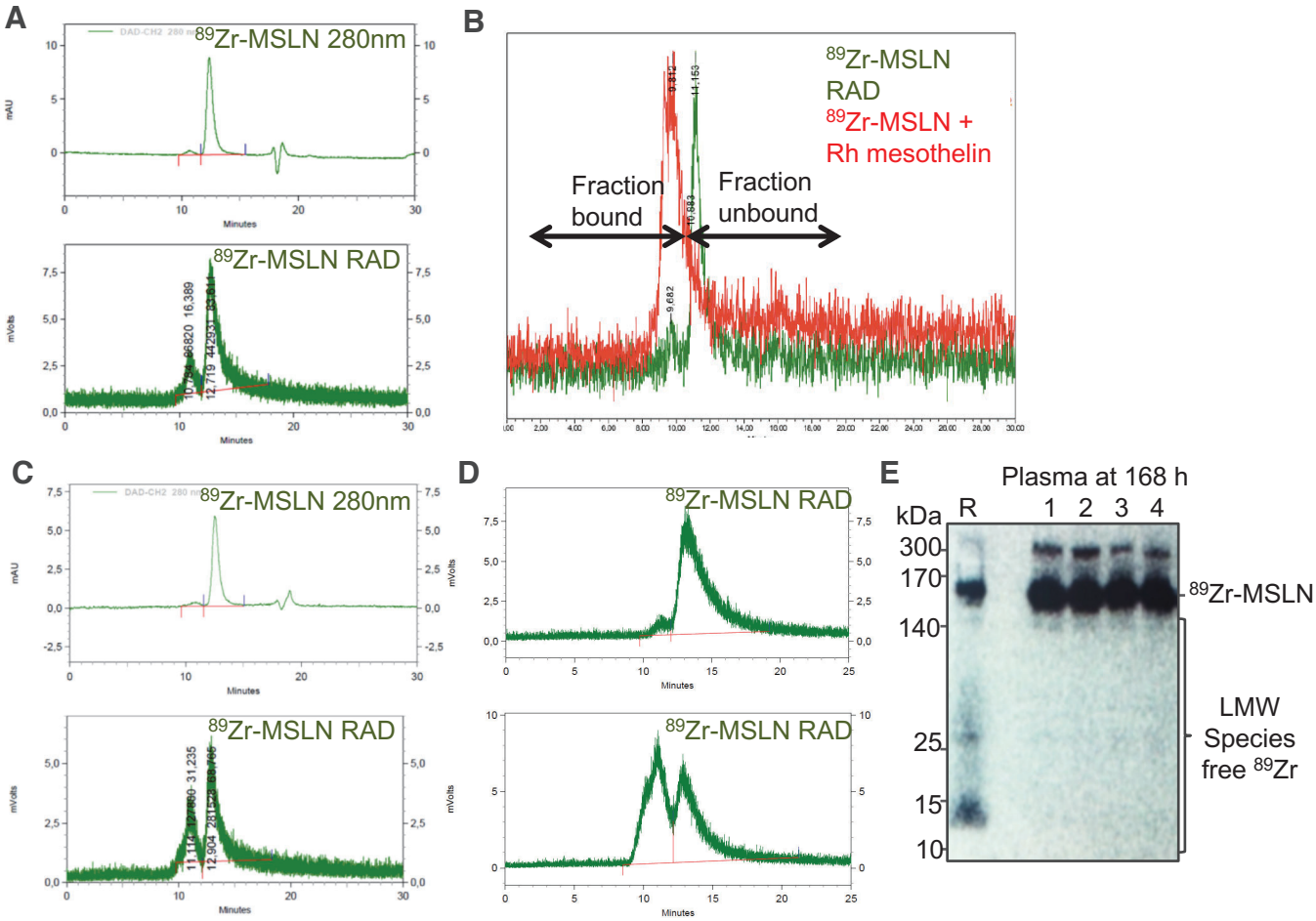

Supplemental Figure 1. ^{89}Zr-MSLN quality control

Ultra-performance liquid chromatography data of **A** optimized ^{89}Zr-MSLN, 4% ± 1% antibody dimers and 15% ± 2% radiolabeled dimers (n = 6) **B** immunoreactive fraction: 0.8 **C** 20 μg ^{89}Zr-MSLN preparation with 30% radioactive dimers **D** ^{89}Zr-MSLN with 10% vs 60% radioactive dimers (at 280 nm ≤5 % data not shown). On y-axis arbitrary units at 280 nm and millivolts at radioactivity detection. **E** *Ex vivo* tracer integrity of ^{89}Zr-MSLN in plasma 168 h pi (n = 4), determined by SDS PAGE, detected by autoradiography, R is ^{89}Zr-MSLN 7 days at RT, including free ^{89}Zr. LMW: low molecular weight. R: reference RAD: radioactivity detection Rh: recombinant human.

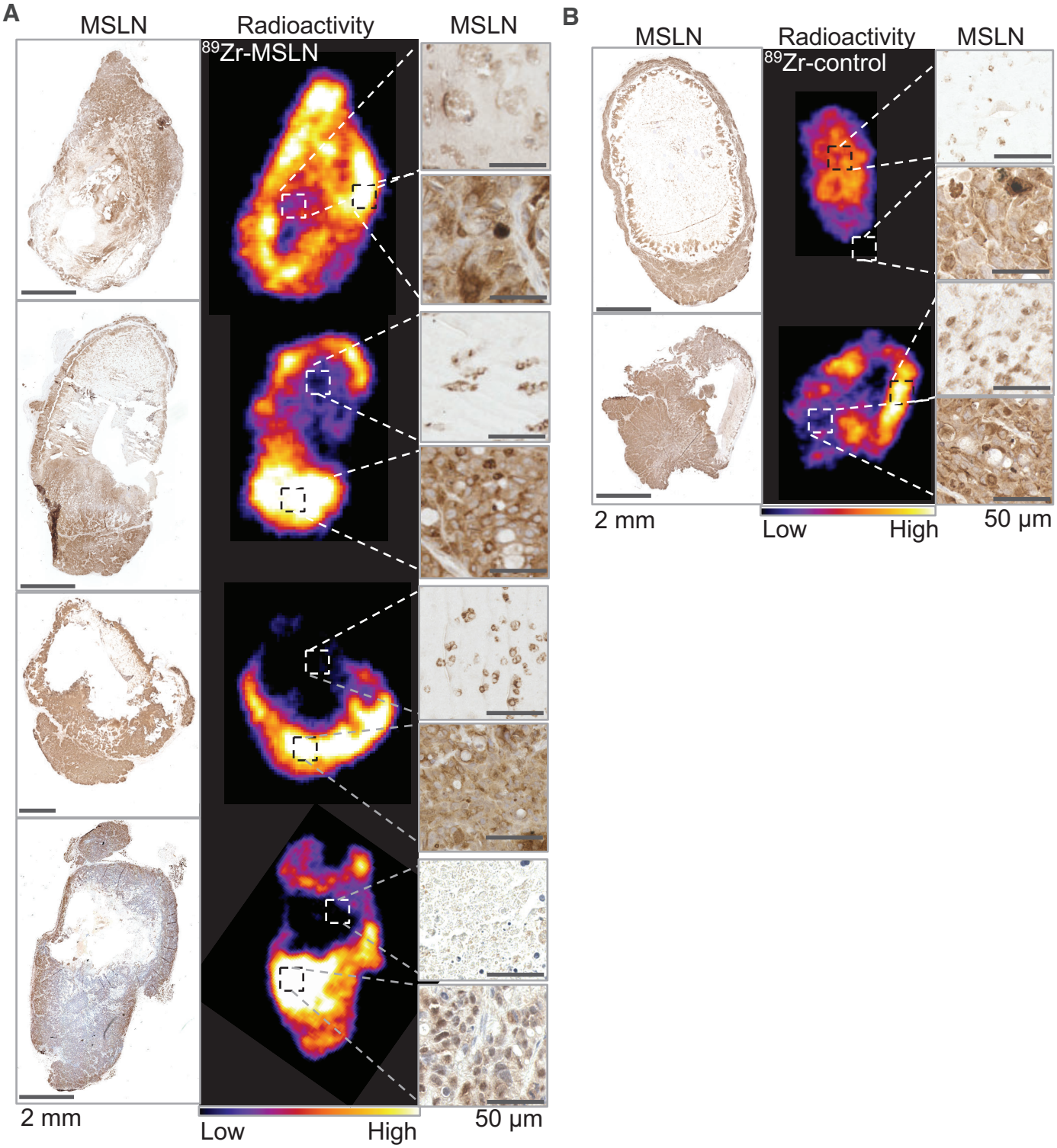

Supplemental Figure 2. Intratumoral ^{89}Zr-MSLN distribution

Mesothelin immunohistochemistry and autoradiography of HT29-MSLN formalin-fixed, paraffin-embedded tumor sections, that received **A** ^{89}Zr-MSLN or **B** ^{89}Zr-control. Mesothelin immunohistochemistry and autoradiography are performed on the same tumor section. Radioactivity is simultaneously scaled in A and B from high to low ^{89}Zr signal intensity. MSLN, Mesothelin.

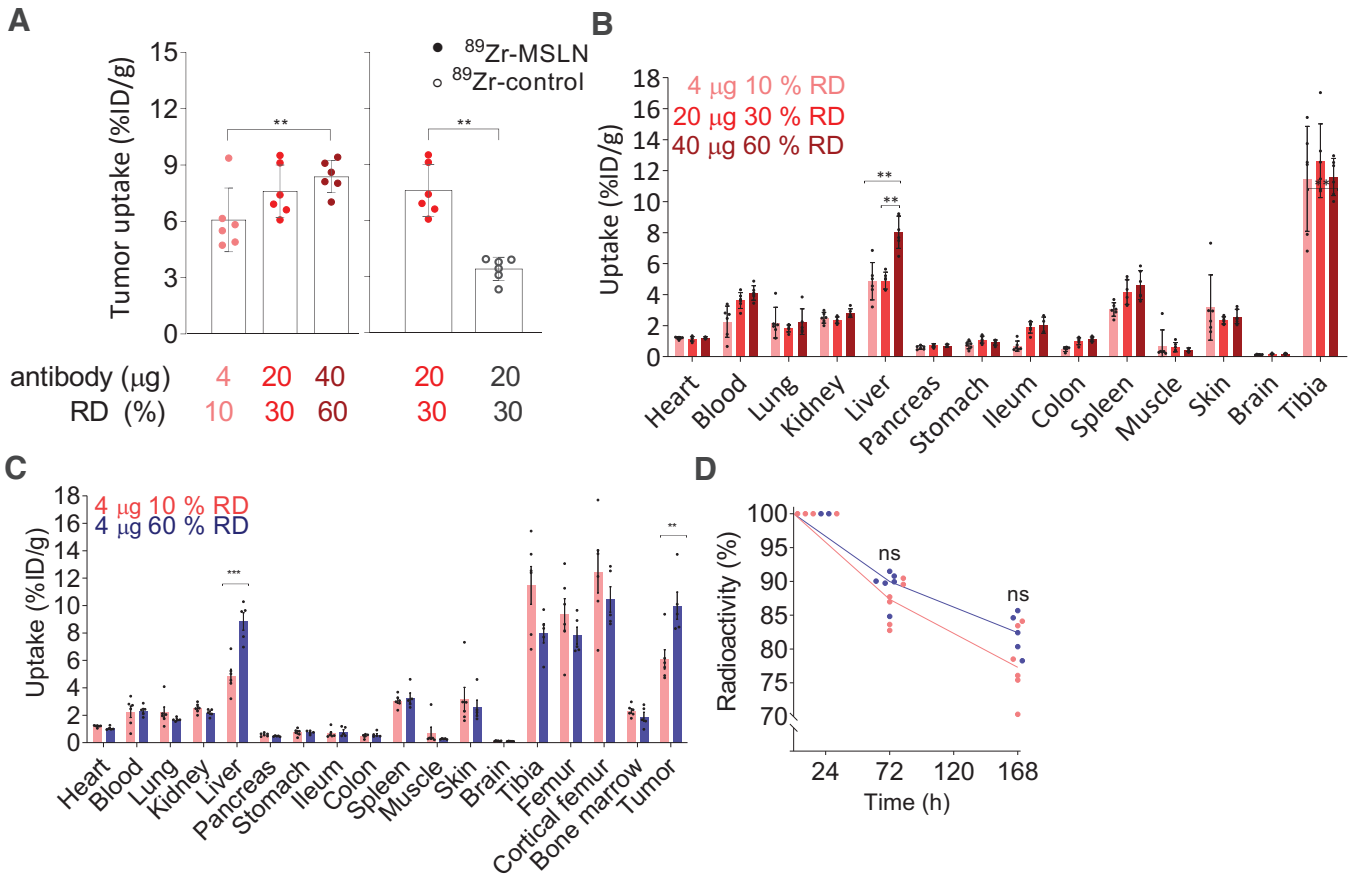

Supplemental Figure 3. Dose- and dimer-effect of ^{89}Zr-MSLN on tumor and healthy tissue uptake

In BxPc3 tumor-bearing mice at 168 h pi **A** *Ex vivo* tumor uptake of 4 µg 10% RD, 20 µg 30% RD, 40 µg 60% RD ^{89}Zr-MSLN and 20 µg 30% ^{89}Zr-control. **B** *Ex vivo* biodistribution of 4 µg 10% RD, 20 µg 30% RD and 40 µg 60% RD ^{89}Zr-MSLN. **C** *Ex vivo* biodistribution of 4 µg ^{89}Zr-MSLN and **D** *in vivo* tracer kinetics, expressed as radioactivity, corrected for decay, with 10% and 60% radioactive dimers. Uptake in tumor and healthy tissues is presented as percentage of injected dose per gram tissue (%ID/g), shown as mean ±SD, including single data points. ***: P <0.001 **: P < 0.01, with Bonferroni conrrection when comparing doses (A). RD: radioactive dimers.

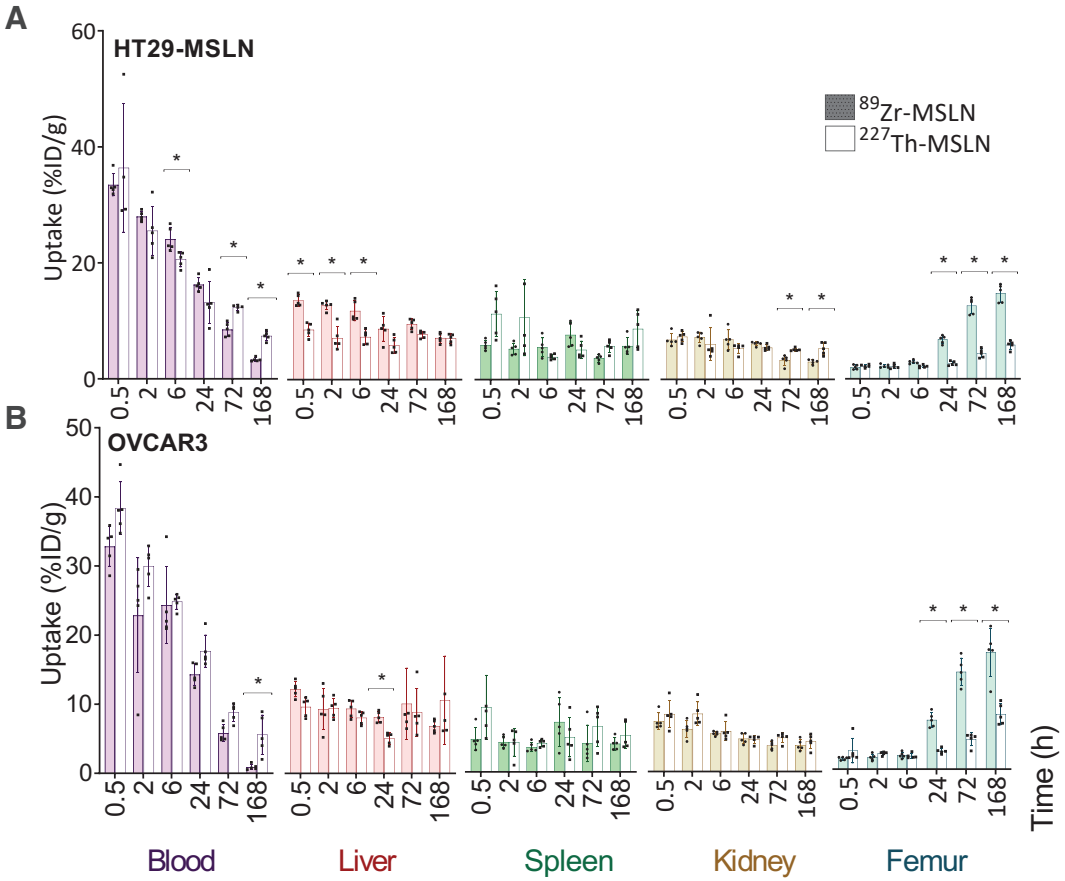

Supplemental Figure 4. ***Ex vivo*** **biodistribution ^{89}Zr-MSLN vs ^{227}Th-MSLN**

in **A** HT29-MSLN tumor-bearing mice and **B** OVCAR3 tumor-bearing mice. Blood levels and uptake in kidney, liver, spleen and intact femur of 20 µg ^{89}Zr-MSLN (0.20 MBq) vs 20 µg ^{227}Th-MSLN (0.015 MBq) at 0.5, 2, 6, 24, 72, and 168 h. Data is presented as mean percentage injected dose per gram tissue (%ID/g) ±SD, including single data points. *: $P < 0.05$ with Bonferroni correction.

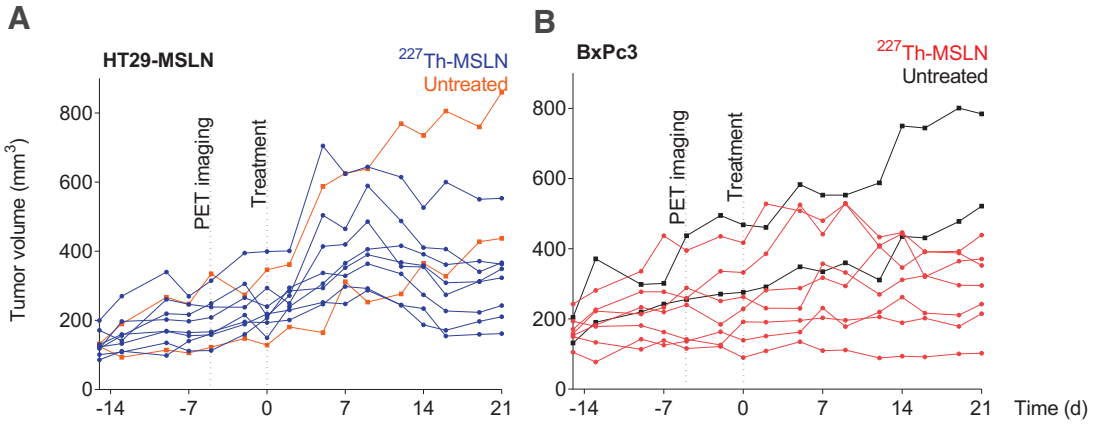

Supplemental Figure 5. Absolute tumor growth after ^{227}Th-MSLN treatment of **A** HT29-MSLN tumor-bearing mice (n = 8) and **B** BxPc3 tumor-bearing mice (n = 7) treated with 0.75 mg/kg 500 kBq/kg ^{227}Th-MSLN and n = 2 untreated mice per model. Tumor volumes expressed as mm^3.

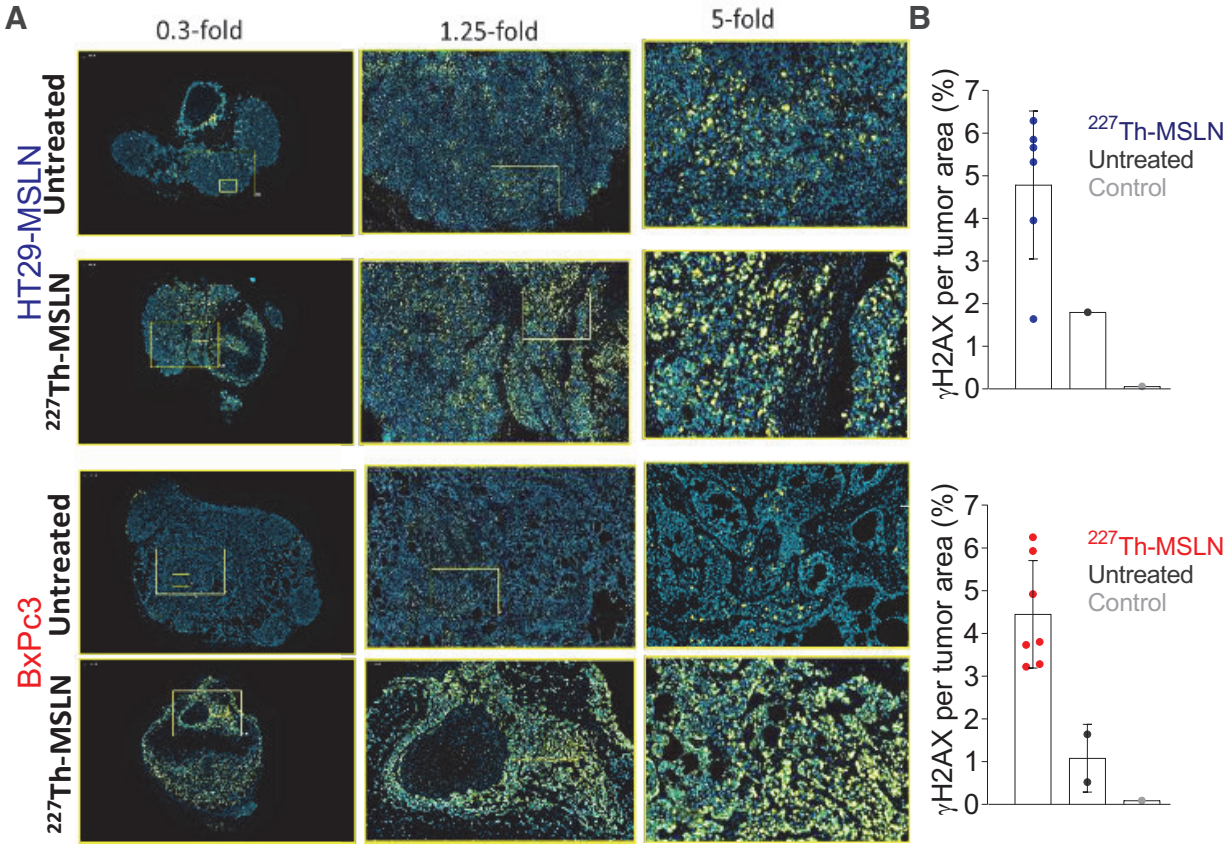

Supplemental Figure 6. γH2AX expression in tumors of mice treated with ^{227}Th-MSLN

A γ H2AX immunofluorescence, marking double-strand DNA breaks, in HT29-MSLN and BxPc3 tumors of 0.75 mg/kg 500 kBq/kg ^{227}Th-MSLN treated (n = 6-7 per group) and untreated mice (n = 1-2 per group) harvested 21 days after injection **B** and quantification expressed as % γH2AX per tumor area. Data are mean ±SD, including single data points. Control: monoclonal mouse IgG2a antibody staining control. γH2AX: gamma H2A histone family member X.

γH2AX immunofluorescence

DNA double-strand breaks were detected with immunofluorescence using a human-specific gamma H2A histone family member X (γH2AX) antibody (Cell Signaling, Clone JBW301, mouse), and a monoclonal mouse IgG2a antibody, clone DAK-GO5 (DAKO) was used as control (dilution 1:2000). Sections were exposed to a Cy3-labeled anti-murine-reactive antibody (Perkin Elmer; Opal™ 4-Color Fluorescent IHC Kit). Tumor sections were counter-stained using DAPI. γH2AX foci were quantified using the HS Analysis Webkit tool (HS Analysis; Karlsruhe Institute of Technology, Germany).

Supplemental Table 1: ^{89}Zr-MSLN development for *in vivo* studies: critical conditions

Optimal conditions ^{89}Zr-MSLN production:	
Buffer exchange method	PD gravity filtration with HEPES 0.5 M pH 6.7
^{89}Zr labeling conditions	0.1 mg/mL MSLN-3,2-HOPO concentration 250-500 MBq/mg specific activity In HEPES buffer
Purification method	PD10 gravity filtration purification, elution with: 10 mM histidine 130 mM glycine buffer pH 7.4
<u>Avoid</u> the following conditions to limit radioactive dimer formation:	
Buffer exchange method	Ultracentrifugation (Vivaspin) or NaCl 0.9%
^{89}Zr labeling condition	> 0.1 mg/mL MSLN-HOPO concentration < 200 MBq/mg specific activity Buffers: • Ammonium acetate pH 7 • Ammonium acetate pH 5.5 • Citrate buffer 30 mM • Addition of cold ^{89}Zr
Purification method	Purification by ultracentrifugation (Vivaspin) PD purification with: • NaCl 0.9% • HEPES 0.5 M pH 7 • EDTA addition before purification • Gentisic acid • Tris buffer pH 8.5 • Sodium phosphate buffer pH 7 • Sodium phosphate buffer pH 8.5 • Histidine glycine 10/130 mM pH 8.5 • Glucose 5% • Arginine glycine 50/50 mM pH 8.5

PD: protein desalting, EDTA: ethylenediamine tetraacetic acid.

Supplemental Table 2: ^{89}Zr-MSLN and ^{227}Th-MSLN batches for *in vivo* studies

	^{89}Zr-MSLN				^{89}Zr-control	^{227}Th-MSLN
Antibody dose (µg)	4	4	20	40	20	20
Radioactive dose (MBq)	1	1	3	3	4	0.015
Radiolabeling efficiency (%)	60	60	64	92	76	99
Antibody concentration (mg/ml)	0.1	0.1	0.2	0.4	0.2	0.2
Specific activity (MBq/mg)	400	400	250	125	250	0.7
Radiochemical purity (%)	99	99	97	99	98	99
Radioactive dimers (%)	10	60	30	60	30	<10
Total antibody dimers (%)	<5	5	5	5	5	<5

Batches of 4 μg and 40 μg ^{89}Zr-MSLN were injected in the BxPc3 tumor-bearing mice (Suppl. Fig. 3), 20 μg ^{89}Zr-MSLN and ^{89}Zr-control were injected in HT29-MSLN tumor-bearing mice (Fig. 1). The 20 μg ^{227}Th-MSLN was injected in HT29-MSLN tumor-bearing mice (Fig. 5).